Cylicins are a structural component of the sperm calyx being indispensable for male fertility in mice and human

Simon Schneider[1,2,†], Andjela Kovacevic[1,†], Michelle Mayer[1,3], Ann-Kristin Dicke[4], Lena Arévalo[1], Sophie A. Koser[4], Jan N. Hansen[5], Samuel Young[6], Christoph Brenker[6] Sabine Kliesch[6], Dagmar Wachten[5], Gregor Kirfel[7], Timo Strünker[6], Frank Tüttelmann[4] and Hubert Schorle[1,*]

[1] Institute of Pathology, Department of Developmental Pathology, Medical Faculty, University of Bonn, 53127 Bonn, Germany

[2] Bonn Technology Campus, Core Facility "Gene-Editing", Medical Faculty, University of Bonn, 53127 Bonn, Germany

[3] Present address: Life and Medical Sciences Institute, Department for Immunology and Environment, University of Bonn, 53115 Bonn, Germany

[4] Institute of Reproductive Genetics, University of Münster, Münster, Germany

[5] Institute of Innate Immunity, Biophysical Imaging, Medical Faculty, University of Bonn, 53127 Bonn, Germany

[6] Centre of Reproductive Medicine and Andrology, University Hospital Münster, University of Münster, Münster, Germany

[7] Institute for Cell Biology, University of Bonn, 53121 Bonn, Germany

[*]correspondence: Hubert.Schorle@ukbonn.de

† contributed equally

Abstract

Cylicins are testis specific proteins which are exclusively expressed during spermiogenesis. In mice and humans, two Cylicins, the gonosomal X-linked Cylicin 1 (*Cylc1/CYLC1*) and the autosomal Cylicin 2 (*Cylc2/CYLC2)* genes have been identified. Cylicins are cytoskeletal proteins with an overall positive charge due to lysine-rich repeats. While Cylicins have been localized in the acrosomal region of round spermatids, they resemble a major component of the calyx within the perinuclear theca at the posterior part of mature sperm nuclei. However, the role of Cylicins during spermiogenesis has not yet been investigated. Here, we applied CRISPR/Cas9 mediated gene-editing in zygotes to establish *Cylc1*- and *Cylc2*-deficient mouse lines as a model to study the function of these proteins. *Cylc1*-deficiency resulted in male subfertility whereas *Cylc2*$^{-/-}$, *Cylc1*$^{-/y}$ *Cylc2*$^{+/-}$, and *Cylc1*$^{-/y}$ *Cylc2*$^{-/-}$ males were infertile. Phenotypical characterization revealed that loss of Cylicins prevents proper calyx assembly during spermiogenesis. This results in decreased epididymal sperm counts, impaired shedding of excess cytoplasm, and severe structural malformations, ultimately resulting in impaired sperm motility. Furthermore, exome sequencing identified an infertile man with a hemizygous variant in *CYLC1* and a heterozygous variant in *CYLC2*, displaying morphological abnormalities of the sperm including the absence of the acrosome. Thus, our study highlights the relevance and importance of Cylicins for

spermiogenic remodeling and male fertility in human and mouse, and provides the basis for further studies on unraveling the complex molecular interactions between perinuclear theca proteins required during spermiogenesis.

Keywords: *Cylc1*, *Cylc2*, Cylicin, male infertility, subfertility, sperm, calyx, perinuclear theca, cytoskeleton, manchette, motility, CRISPR, gene-editing

Introduction

The differentiation of round spermatids into sperm during spermiogenesis is a highly organized and spatiotemporally controlled process taking place in the seminiferous epithelium of the testis. Cellular and morphological remodeling involves DNA hypercondensation, establishment of a species-specific head morphology, removal of excess cytoplasm as well as formation of accessory structures like acrosome and flagellum. These structural changes depend on a highly efficient protein trafficking machinery and a unique sperm cytoskeleton [1]. One essential cytoskeletal element is the perinuclear theca (PT), which surrounds the sperm nucleus, except for the caudal edge, at the implantation site of the flagellum. The PT is supposed to serve as a structural scaffold for the sperm nucleus and resembles a rigid cytosolic protein layer, which is resistant to non-ionic detergents and high salt buffer extractions [2, 3]. The PT has been subdivided into a subacrosomal and postacrosomal part based on its localization, function, composition, and developmental origin. The subacrosomal part of the PT develops early during spermiogenesis, simultaneously with the formation of the acrosome. It is supposed to emerge from acrosomal vesicles, and presents as a thin cytosolic protein layer between the inner acrosomal membrane and the nuclear envelope [4, 5]. The postacrosomal part of the PT, also known as the sperm calyx, originates from cytosolic proteins that are transported via the manchette and assembled during sperm head elongation [4]. It is located in between the nuclear envelope and the sperm plasma membrane.

Proteomic analyses using murine and bovine PT extracts revealed 500-800 different proteins, highlighting its high molecular complexity [6, 7]. Apart from cytoskeletal proteins, signaling molecules and several *de novo* synthesized core histones were identified. They are proposed to be essential for sperm-egg interaction and chromatin remodeling of the male pronucleus at early post-fertilization stages [8, 9, 4, 10, 11]. Many structural proteins of the PT are testis-specific and uniquely expressed in the PT, including Calicin (*Ccin*) [12, 2, 13], Cylicin 1 (*Cylc1*) and Cylicin 2 (*Cylc2*) [2, 14, 15], actin-capping proteins CPβ3 and CPα3 [16–18] as well as actin-related proteins Arp-T1 and Arp-T2 [19]. Despite being characterized on molecular level, their function remains largely elusive.

73 Both, *Ccin* and Cylicins are highly basic proteins with a predominant localization in the calyx of mature
74 sperm [14, 15, 12]. In most species, two Cylicin genes, *Cylc1* and *Cylc2*, have been identified. They are
75 characterized by repetitive lysine-lysine-aspartic acid (KKD) and lysin-lysin-glutamic acid (KKE) peptide
76 motifs, resulting in an isoelectric point (IEP) > pH 10 [14, 15]. While the *CYLC2/Cylc2* gene is encoded on
77 autosomes, the human and murine *CYLC1/Cylc1* gene is encoded on the X-chromosome, resulting in
78 hemizygosity in males. Further, in bovine, Cylc2 serves as actin-binding protein of the sperm
79 perinuclear cytoskeleton [20]. Cylicins seem to be cytoskeletal regulators and required for proper sperm
80 head architecture.

81 In this study, we report the CRISPR/Cas9-mediated generation and characterization of *Cylc1-*, *Cylc2-,*
82 and *Cylc1/2*-deficient mice, demonstrating that Cylicins are indispensable for male fertility and play a
83 key function in the formation of the sperm calyx. We show that Cylicins are required for the
84 maintenance of the PT integrity during spermiogenesis and in mature sperm. Their deficiency results
85 in morphological defects of the sperm head, acrosome, and mid-piece. Our analyses revealed that
86 *Cylicin* genes are evolutionary conserved in rodents and primates. Furthermore, we identified Cylicin
87 variants in an infertile man, demonstrating the conserved role of Cylicins in regulating male infertility.

88

89 **Results**

90 **Cylicins are indispensable for male fertility in mice**

91 Cylicins were first discovered and characterized in the early nineties, and a role in sperm head
92 architecture was postulated due to their subcellular localization [2, 14, 15], however, any functional
93 evidence has been lacking. To address the question of the role of Cylicins during spermiogenesis, we
94 used CRISPR/Cas9-mediated gene-editing to generate *Cylc1* and *Cylc2* deficient mouse models. First,
95 for *Cylc1*, a pair of sgRNAs targeting exon 5 was designed, and a mouse line with a frameshift inducing
96 deletion of 1.585 kb, accounting for 85% of the *Cylc1* coding sequence, was established. Next, two
97 guide RNAs targeting exon 4/5 of the *Cylc2* gene were applied to establish a *Cylc2* deficient mouse line
98 with a 1.145 kb frameshift inducing deletion (Fig. 1 A). In both lines, the majority of predicted
99 functional domains with repetitive, lysine-lysine-aspartic acid (KKD) and lysin-lysin-glutamic acid (KKE)
100 peptide motifs were depleted. Depletion was confirmed by PCR-based genotyping (Fig. 1 B).

101 Fertility testing of *Cylc1*$^{-/y}$ males revealed significantly reduced pregnancy rates (16 %) and mean litter
102 size (2.2) (Fig. 1 C). *Cylc2*$^{-/-}$ males were infertile, while *Cylc2*$^{+/-}$ males showed no significant difference
103 in fertility parameters compared to wildtype mice (Fig. 1 C). Additionally, established mouse lines were
104 intercrossed to generate *Cylc1*$^{-/y}$ *Cylc2*$^{+/-}$ and *Cylc1*$^{-/y}$ *Cylc2*$^{-/-}$ males. Of note, *Cylc1*$^{-/y}$ *Cylc2*$^{+/-}$, and *Cylc1*$^{-/y}$
105 *Cylc2*$^{-/-}$ males were infertile (Fig. 1 C). This indicates that loss of *Cylc1* alone is partially tolerated, as
106 suggested by subfertility of Cylc1$^{-/y}$ males, whereas the additional loss of one *Cylc2* allele renders male

107 mice infertile. Taken together, the results suggest, that two functional Cylicin alleles are required for
108 male fertility.

109 qRT PCR confirmed the absence of *Cylc1* and/or *Cylc2* transcripts in Cylicin-deficient animals (Fig. 1 D).
110 For *Cylc2*$^{+/-}$ animals a gene-dosage effect was observed, as indicated by a 50 % reduced *Cylc2*
111 expression. Neither loss of *Cylc1* nor *Cylc2* resulted in upregulation of *Cylc2* or *Cylc1*, respectively.

112 Next, due to the lack of commercial antisera, polyclonal antibodies against murine CYLC1 and CYLC2
113 were raised to visualize the localization of Cylicins during spermiogenesis. Immunofluorescence
114 staining of wildtype testicular tissue showed presence of both, CYLC1 and CYLC2 from the round
115 spermatid stage onward (Fig. 1D, E). The signal was first detectable in the subacrosomal region as a
116 cap like structure, lining the developing acrosome (Fig. 1D, E). As the spermatids elongate, CYLC1 and
117 CYLC2 move across the PT towards the caudal part of the cell (Fig. S1 A). At later steps of
118 spermiogenesis, the localization in the subacrosomal part of the PT faded while it intensified in the
119 postacrosomal calyx region. (Fig. 1 D, E). Of note the localization of CYLC1 and CYLC2 in the calyx of
120 mature sperm has been reported in bovine and human [14, 15, 20]. The generated antibodies did not stain
121 testicular tissue and mature sperm of *Cylc1*- and *Cylc2*-deficient males demonstrating i) specificity of
122 the antibodies and ii) validating the knockout mice (Fig. 1 E).

123 Next, spermiogenesis of Cylicin-deficient males was analyzed in detail. Gross testicular morphology as
124 well as testicular weight were not significantly altered (Fig. 2 A, B). The testicular morphology appeared
125 unaltered, with all stages of spermatogenesis being detectable in PAS-stained testicular sections (Fig.
126 2 C). However, a strong decline in cauda epididymal sperm counts was observed in all Cylicin-deficient
127 males. For *Cylc1*$^{-/y}$ and *Cylc2*$^{+/-}$ males, a moderate reduction of 40-47% was determined, whereas
128 *Cylc2*$^{-/-}$ and *Cylc1*$^{-/y}$ *Cylc2*$^{+/-}$ displayed an approx. 65% reduction in epididymal sperm counts compared
129 to wildtype mice (Fig. 2 D). In *Cylc1*$^{-/y}$ *Cylc2*$^{-/-}$ males, spermiogenesis was most impaired, as indicated
130 by an 85% reduction of the sperm count (Fig. 2 D). Eosin-nigrosine staining revealed that the viability
131 of epididymal sperm from all genotypes was above the lower reference limit of 58% (Fig. 2 E, Fig. S1
132 B). However, viability of *Cylc2*$^{-/-}$ and *Cylc1*$^{-/y}$ *Cylc2*$^{-/-}$ sperm was reduced by approx. 15% compared to
133 wildtype sperm. (Fig. 2 E). The motility of *Cylc1*$^{-/y}$ and *Cylc2*$^{+/-}$ sperm remained unchanged compared
134 to wildtype sperm (around 60% motile cells), whereas motility of *Cylc2*$^{-/-}$ sperm was drastically reduced
135 to only 7% motile sperm (Fig. 2 F) and the motility of *Cylc1*$^{-/y}$ *Cylc2*$^{-/-}$ sperm was reduced to 2% motile
136 sperm. In addition, the few motile sperm cells were not progressive but were swimming in circular
137 trajectories. Interestingly, in *Cylc1*$^{-/y}$ *Cylc2*$^{+/-}$ mice, sperm motility was reduced as well, but less
138 drastically, with 27% of sperm cells being motile (Fig. 2 F).

139

140 ***Cylc2*$^{-/-}$ sperm cells have altered flagellar beat**

141 The SpermQ software was used to analyze the flagellar beat of *Cylc2*$^{-/-}$ sperm in detail [21]. *Cylc2*$^{-/-}$ sperm
142 showed stiffness in the neck and a reduced amplitude of the initial flagellar beat, as well as reduced
143 average curvature of the flagellum during a single beat (Fig. S4 A). Interestingly, we observed that the
144 flagellar beat of *Cylc2*$^{-/-}$ sperm cells was similar to wildtype cells with - however – interruptions during
145 which midpiece and initial principal piece appeared stiff whereas high frequency beating occurs at the
146 flagellar tip (Fig. 2G, supplementary Video 1, supplementary Video 2). These interruptions occurred
147 only on the open-hook side and the duration of such interruptions varied from beat to beat. As these
148 anomalies introduce a high asymmetry to the flagellar beating, swimming of such sperm is very likely
149 perturbed limiting the capability to reach the egg [22]. Of note similar phenotypes have been observed
150 for sperm with structural defects in the axoneme [22]. Thus, we hypothesized that there may be
151 structural defects in *Cylc2*-deficient sperm.

152

153 **Sperm morphology is severely altered in Cylicin deficient mice**

154 Indeed, transmission electron microscopy (TEM) of epididymal sperm revealed that *Cylc2*-deficiency
155 causes severe structural defects (Fig. 3 A, Fig. S2 A): *Cylc2*$^{-/-}$ sperm showed coiling of the tail and
156 dislocation of the tail connecting piece from the basal plate, resulting in parallel position of head and
157 tail (Fig. 3 A, white arrowheads). The coiling of the flagellum was also observed using bright field
158 microscopy (Fig. S2 B). Furthermore, in *Cylc2*$^{-/-}$ sperm, excess of cytoplasm was observed, located
159 around the nucleus and coiled tail (Fig. 3 A). Anomalies of the head were observed at the level of the
160 PT, while the nuclei appeared unaltered. In all *Cylc2*$^{-/-}$ sperm cells, the posterior portion of PT – calyx
161 was absent (Fig. 3 A, red arrowheads). Instead of surrounding the nucleus entirely, the PT in *Cylc2*$^{-/-}$
162 sperm appeared interrupted, missing completely its caudal part. Further, we observed loosening of
163 the peri-acrosomal region, which is not compact and adherent to the nucleus (Fig. 3 A, green
164 arrowheads). Although the axoneme structure appeared unaltered, presenting typical 9+2
165 microtubular composition, many *Cylc2*$^{-/-}$ sperm cells had damaged mitochondria (Fig. S2 A).

166 Next, we used PNA-FITC lectin immunofluorescence staining to analyze acrosome localization in
167 mature sperm, as well as MITOred to visualize mitochondria in the flagellum (Fig. 3 B, C). Loss of *Cylc1*
168 alone caused malformations of the acrosome in around 42% of mature sperm, while their flagellum
169 appeared unaltered and properly connected to the head. While *Cylc2*$^{+/-}$ males showed normal sperm
170 morphology, 94% of *Cylc2*$^{-/-}$ mature sperm cells displayed morphological alterations of head and mid-
171 piece (Fig. 3 B, C). *Cylc2*$^{-/-}$ sperm cells showed acrosome malformations, bending of the neck region,
172 and/or coiling of the flagellum, occasionally resulting in its wrapping around the sperm head (Fig. 3 B).

173 While 75% of *Cylc1*$^{-/Y}$ *Cylc2*$^{+/-}$ sperm showed these morphological alterations, 99% of *Cylc1*$^{-/Y}$ *Cylc2*$^{-/-}$
174 sperm presented with coiled tail and abnormal acrosome (Fig. 3 B, C).

175 **Loss of Cylicins prohibits calyx assembly during spermiogenesis**

176 Since TEM micrographs revealed absence of calyx in *Cylc2*$^{-/-}$ epididymal sperm (Fig. 3 A, red
177 arrowheads), we analyzed the localization of other calyx specific proteins, such as CCIN and CapZα3. In
178 *Cylc*1$^{-/y}$ and *Cylc2*$^{+/-}$ sperm, CCIN localization remained unchanged, being present in the calyx and in
179 the ventral portion of PT as described previously [7]. However, in *Cylc2*$^{-/-}$ sperm, CCIN localizes to the tail
180 or in random parts of the sperm head (Fig. 3 D). In *Cylc1*$^{-/Y}$ *Cylc2*$^{+/-}$ and *Cylc1*$^{-/Y}$ *Cylc2*$^{-/-}$ sperm, the
181 localization of CCIN was also altered, with the signal mainly being present in the sperm tail. CapZα3
182 forms a heterodimer with CapZβ3, creating a functional complex that localizes in the calyx [23].
183 Immunofluorescence stainings revealed that the localization of CapZα3 remained unchanged in *Cylc1*$^{-/Y}$
184 and *Cylc2*$^{+/-}$mice compared to wildtype mice. In many *Cylc2*$^{-/-}$ sperm cells, CapZα3 localizes in the caudal
185 portion of the head but without regular calyx localization (Fig. 3 D). Interestingly, *Cylc1*$^{-/Y}$ *Cylc2*$^{+/-}$ mice
186 showed less severe anomalies of the calyx and although CCIN is located almost exclusively in the tail,
187 CapZα3 maintains the correct calyx localization (Fig. 3 D). Finally, *Cylc1*$^{-/Y}$ *Cylc2*$^{-/-}$ spermatozoa showed
188 CapZα3 localization across the sperm head without regular calyx shape. These results suggest that the
189 loss of Cylicins impairs the formation of calyx and the correct localization of its components, which
190 might cause further morphological anomalies of the sperm (Fig. 3 D).

191

192 **Loss of *Cylc2* impairs sperm nuclear morphology**

193 To analyze in detail the sperm head, we used Nuclear Morphology software on DAPI stained sperm
194 samples. *Cylc1*$^{-/Y}$ and *Cylc2*$^{+/-}$ sperm showed no alterations of the nuclear shape when compared to
195 wildtype (Fig. 3 E, Fig. S2C, D). However, heads of *Cylc2*$^{-/-}$ and *Cylc1*$^{-/Y}$ *Cylc2*$^{-/-}$ sperm appeared smaller,
196 with shorter hooks and increased circularity of the nuclei as well as reduced elongation (Fig. 3 E, Fig.
197 S2D). This indicates that loss of *Cylc2* causes a mild globozoospermia. Interestingly, *Cylc1*$^{-/Y}$ *Cylc2*$^{+/-}$
198 sperm heads were not drastically altered, suggesting that only *Cylc2* has a crucial role for sperm head
199 shaping, and one functional *Cylc2* allele is sufficient to maintain the correct shape of the nucleus (Fig.
200 3 E, Fig. S2D). Furthermore, the head of many *Cylc2*-deficient sperm appeared less concave at the
201 region proximal to the connecting piece (Fig. 3 E).

202

203

204 **Cylicins are required for acrosome attachment to the nuclear envelope**

205 PNA lectin staining of testicular tissue sections was performed to investigate acrosome biogenesis.
206 During Golgi phase, the acrosome first starts to appear as an aggregation of proacrosomal vesicles into
207 a single granule. This premature acrosomal structure was unaltered in all genotypes, with PNA signal
208 appearing as a small dot on one pole of round spermatids (Fig. 3 F). During cap phase, acrosome grows
209 to cover the apical part of the nucleus. In wildtype and *Cylc2*$^{+/-}$ mice, the forming acrosome appears
210 equally smooth and shows a regular cap structure on the perinuclear region of round spermatids.
211 However, in some of the round spermatids from *Cylc2*$^{-/-}$ and *Cylc1*$^{-/Y}$ mice, gaps in the forming
212 acrosome are observed, as well as an irregular shape of the cap. In *Cylc1*$^{-/Y}$ *Cylc2* $^{+/-}$ and *Cylc1*$^{-/Y}$ *Cylc2*$^{-/-}$
213 mice, most of the round spermatids were deformed or displayed irregularly localized caps (Fig. 3 F, Fig.
214 S3A). At acrosome phase, many elongating spermatids of *Cylc1*$^{-/Y}$, *Cylc2*$^{-/-}$, *Cylc1*$^{-/Y}$ *Cylc2*$^{+/-}$ and *Cylc2*$^{-/-}$
215 *Cylc1*$^{-/Y}$ mice have irregular acrosome (Fig. 3 F, Fig. S3A). Detachment of the acrosome from the nuclear
216 envelope is evident in testis samples of *Cylc2*$^{-/-}$ and *Cylc1*$^{-/Y}$ *Cylc2*$^{-/-}$ male mice. These results suggest
217 that Cylicins are required for the attachment of the developing acrosome to the nuclear envelope
218 during spermiogenesis.

219

220 **Cylicin-deficiency results in abnormal manchette elongation and disassembly**

221 Next, we investigated the role of Cylicins during formation and development of the manchette – a
222 sperm-specific, transient structure that represents a microtubular platform for protein transport.
223 Transport of the intracellular vesicles is crucial for the formation of the flagellum, acrosome assembly
224 and removal of excess cytoplasm. The manchette is first detected at step 8 at the perinuclear ring of
225 round spermatids, just prior to their elongation. During the next steps of spermiogenesis, as the
226 spermatids elongate, manchette moves towards the neck region in a skirt-like structure and starts
227 disassembling at step 13 when the elongation is complete [24]. We used immunofluorescence staining
228 of acetylated α-tubulin on squash testis samples containing spermatids at different stages of
229 spermiogenesis to investigate whether the altered head shape, calyx structure, and tail-head
230 connection anomalies originate from possible defects of the manchette structure. Spermatids starting
231 from stage 8 were observed individually for step-to-step comparison. In all genotypes, a cap-like shape
232 of the manchette was observed in step 8 round spermatids, suggesting that the manchette assembles
233 properly and starts elongating towards the neck region during step 9 (Fig. S3 B). In all genotypes, the
234 typical skirt-like structure was observed at the caudal region of the spermatids at step 10 and 11,
235 suggesting that the manchette assembles correctly even in Cylicin-deficient sperm (Fig. 4 A). In
236 spermatids from *Cylc1*$^{-/Y}$ and *Cylc2*$^{+/-}$ mice, regular manchette development was observed in further
237 steps of spermiogenesis (Fig. 4 A). However, starting from step 12, spermatids from *Cylc2*$^{-/-}$, *Cylc1*$^{-/Y}$

238 *Cylc2*$^{+/-}$, and *Cylc1*$^{-/Y}$ *Cylc2*$^{-/-}$ mice showed abnormal manchette elongation, which became more
239 prominent at step 13 (Fig. 4 A). Interestingly, some of *Cylc2*-deficient spermatids showed shifting of
240 the manchette to the ventral side of the nucleus along with excessive elongation. At step 16, the
241 manchette was normally disassembled in wildtype, *Cylc1*$^{-/Y}$, and *Cylc2*$^{+/-}$ spermatids (Fig. 4 A). However,
242 *Cylc2* $^{-/-}$, *Cylc1*$^{-/Y}$ *Cylc2*$^{+/-}$, and *Cylc1*$^{-/Y}$ *Cylc2*$^{-/-}$ spermatids showed a persistent α-tubulin signal, indicating
243 that disassembly of the manchette is delayed or incomplete (Fig. 4 A).

244 Other than α-tubulin, we also used HOOK1 as manchette marker. HOOK1 is a member of a family of
245 coiled-coil proteins, which bind to microtubules and organelles and regulate microtubule trafficking
246 during endocytosis and spermiogenesis [25]. Co-staining of the spermatids with antibodies against PNA
247 lectin and HOOK1 revealed that abnormal manchette elongation and acrosome anomalies
248 simultaneously occurred in elongating spermatids of *Cylc2*$^{-/-}$ male mice (Fig. 4 B): While manchette was
249 moving excessively towards the tail, the developing acrosome lost its compact adherence to the
250 nuclear envelope (Fig. 4 B), causing the concomitant anomalies in the mature sperm. Schematic
251 representation shows acrosome biogenesis and manchette development in wildtype and *Cylc2*$^{-/-}$
252 spermatids (Fig. 4 B). While round spermatids of *Cylc2*$^{-/-}$ mice elongated as those of the wildtype sperm,
253 the manchette elongated abnormally and the acrosome became loosened (Fig. 4 B).

254 Transmission electron microscopy of testicular tissues of wildtype and *Cylc2*$^{-/-}$ mice showed detailed
255 structure of spermatids at different steps of spermiogenesis (Fig. 4 C). Round spermatids at step 6
256 showed correct assembly of the proacrosomal granule typical for Golgi phase, as well as normal looking
257 PT in both wildtype and *Cylc2*$^{-/-}$ mice (Fig. 4 C). However, in *Cylc2*$^{-/-}$ elongating spermatids already at
258 step 8, we observed wide gaps in the PT at the perinuclear ring level, between the growing acrosome
259 (Fig. 4 C, green arrowheads) and the developing manchette (Fig. 4 C, red arrowheads; gaps are depicted
260 by dashed line). In wildtype spermatids, these structures were in close contact (Fig. 4 C). Acrosome
261 biogenesis proceeded regularly with acrosomal caps forming at the apical pole of the spermatids. At
262 step 9-10 spermatids of *Cylc2*$^{-/-}$ mice we already observed manchette anomalies. In many cells,
263 microtubules appeared longer on one side of the nucleus than on the other, displacing the acrosome
264 to the side. In turn, this might result in abnormal attachment of the developing flagellum to the basal
265 plate and consequently flipping of the head and coiling of the tail in mature spermatozoa (Fig. 4 C). At
266 step 11-12, excessive elongation of the manchette in *Cylc2*$^{-/-}$ spermatids as well as the gaps in PT were
267 observed. Whereas elongated spermatids at step 14-15 in wildtype sperm already disassembled their
268 manchette and the PT appeared as a unique structure that compactly surrounds nucleus, in *Cylc2*$^{-/-}$
269 spermatids, remaining microtubules failed to disassemble, and the acrosome detached from the
270 nuclear envelope. In addition, at step 16, the calyx was absent, and an excess of cytoplasm surrounded
271 the nucleus and flagellum (Fig. 4 C, yellow arrowhead). Furthermore, many damaged and degrading

272 cells were observed in testicular tissue TEM samples, having perforated nuclei and detached structures
273 (Fig. 4 D). Interestingly, phagosomes with cellular remains were observed far away from the lumen and
274 sometimes even at the basal membrane of the tubuli, suggesting that the cells that suffer most severe
275 structural damage are being removed. This mechanism of removing malformed cells explains the
276 reduction of epididymal sperm count in Cylicin-deficient genotypes.

277 We conclude that loss of two Cylicin alleles does not disturb the initial phase of manchette formation
278 but causes the delocalization of the manchette towards the tail and abolishes timely manchette
279 disassembly. The localization of manchette on the caudal portion of spermatids coincides with the
280 localization of the calyx in the mature sperm, so these results indicate that the manchette might be
281 maintained longer to compensate for the missing formation of the calyx structure.

282

283 ***Cylc2* coding sequence is slightly more conserved among species than *Cylc*1**

284 To address why *Cylc2* deficiency causes more severe phenotypic alterations than *Cylc1*-deficiency in
285 mice, we performed evolutionary analysis of both genes. Selective pressures on protein level were
286 represented by calculation of the nonsynonymous/synonymous substitution rate ratio ($\omega = dN/dS$). It
287 distinguishes between purifying selection ($\omega<1$), neutral evolution ($\omega=1$) and positive selection ($\omega>1$).
288 Analysis of the selective constrains on *Cylc1* and *Cylc2* across rodents and primates revealed that both
289 genes' coding sequences are under purifying selection in general, although conservation is weaker in
290 *Cylc1* trending towards a more relaxed constraint (Fig. S4 A, Table S1). For *Cylc1*, the evolutionary rate
291 (ω) of the whole sequence for the whole tree analyzed was significantly lower than, but close to 1 at
292 $\omega=0.85$. For *Cylc2*, it was lower at $\omega=0.49$ (see Table S1). A model allowing for separate calculation of
293 the evolutionary rate for primates and rodents, did not detect a significant difference between the
294 clades, neither for *Cylc1* nor for *Cylc2*, indicating that the sequences are equally conserved in both
295 clades.

296 To analyze the selective pressure across the coding sequence in more detail, we calculated the
297 evolutionary rates for each codon site across the whole tree. The model allowing for positive selection
298 on codon sites explained the data significantly better than the null model according to likelihood ratio
299 analysis (see Table S1). For *Cylc1*, 34% of codon sites were assigned to the conserved site class, 51% to
300 the neutral/relaxed constraint site class, and 15% to the positive selection site class. For *Cylc2*, 47% of
301 codon sites were assigned to the conserved site class, 44% to the neutral/relaxed constraint site class,
302 and 9% to the positive selection site class. Of the codon sites assigned to the positive selection site
303 class three sites were significantly positively selected for *Cylc1* and 11 for *Cylc2* (Table S1). The
304 distribution of evolutionary rates across the sequence revealed largely relaxed constraint in the N-

305 terminal region with several sites of positive selection and purifying selection with positive selection
306 hot spots in the C-terminal region of *Cylc1*. The N-terminal region of *Cylc2* seems to be largely
307 conserved with a pattern of conservation and stronger positive selection in the internal and C-terminal
308 region. Interestingly, codon sites encoding lysine residues, which are proposed to be of functional
309 importance for Cylicins, are mostly conserved. For *Cylc1*, 17% of lysine residues are significantly
310 conserved and 35% of significantly conserved codons encode for lysine. For *Cylc2*, this pattern is even
311 more pronounced with 27.9% of lysine codons being significantly conserved and 24.3% of all conserved
312 sites encoding for lysine (Fig. S4).

313

314 **Cylicins are required for normal sperm morphology in human**

315 As loss of two Cylicin alleles causes fertility defects in mice, we next addressed whether infertile men
316 also display variants in *CYLC1/CYLC2*.

317 Exome sequencing within the MERGE (**M**al**e** **R**eproductive **G**enomics study) cohort identified one
318 patient (M2270) carrying rare (MAF < 0.01, gnomAD) missense variants in both *CYLC1* and *CYLC2*. The
319 hemizygous variant c.1720G>C in *CYLC1* leads to an amino acid exchange from glutamic acid to
320 glutamine (p.(Glu574Gln)) which is predicted to be deleterious or possibly damaging by *in silico* tools
321 (SIFT [26] and PolyPhen [27], respectively) and has a CADD score of 11.91. It is located in exon four out of
322 five and affects a region that is predicted to be intolerant to such substitutions (Figure S5, metadome).
323 It occurs only twice in the gnomAD database (v2.1.1) comprising 141,456 individuals (67,961 XY), once
324 identified in a hemizygous male and once in a female carrier, and is absent from our in house database.

325 The heterozygous variant c.551G>A in *CYLC2* is predicted to be tolerated (SIFT) or benign (PolyPhen)
326 which is in accordance with a low CADD score of 0.008. It is located in exon five out of eight and affects
327 a region in which variants are likely to be tolerated (Figure S5, metadome). However, it is a rare variant
328 occurring with an allele frequency of 0.0035 in the general population, according to the gnomAD
329 database. Importantly, only three XX individuals are reported to be homozygous for the variant within
330 *CYCL2*.

331 Segregation analyses revealed maternal inheritance of the X-linked *CYLC1* variant c.1720G>C p.
332 (Glu574Gln), whereas the father carries the heterozygous *CYLC2* variant c.551G>A p.(Gly184Asp) (Fig.
333 5A). According to ACMG-AMP criteria [28] both variants are classified as variants of uncertain significance
334 (Table S2). No other potentially pathogenic variants in genes associated with sperm morphological
335 defects were identified by exploring the exome data of M2270.

336 Semen analysis performed following WHO guidelines [29] is shown in Table 1. The sperm concentration
337 in the semen was slightly reduced, while significant reduction of motile spermatozoa (12.5%) was

338 observed. Interestingly, only 2% of the sperm cells appeared morphologically normal, while 98% of
339 sperm showed head defects (Table 1). Immunofluorescence staining of CYLC1 revealed that while in
340 healthy donor's sperm, CYLC1 localizes in the calyx, in M2270, CYLC1 labeling was absent (Fig. 5B).
341 Bright field microscopy demonstrated that M2270's sperm flagella coiled similarly to that in Cylicin
342 deficient murine sperm samples. Interestingly, DAPI staining revealed that many flagella carry
343 cytoplasmatic bodies without nuclei and could be defined as headless spermatozoa (Fig. 5C). CCIN
344 staining demonstrated that while spermatozoa of a healthy donor showed a typical, funnel-like calyx
345 structure in the posterior region of PT, spermatozoa from M2270 had CCIN localized in irregular
346 manner throughout head and tail, suggesting that Cylicins have a role in maintenance of the calyx
347 structure and composition in both mice and human spermatozoa (Fig. 5D).

348

349 **Discussion**

350 Spermiogenesis is a highly organized process that is dependent on a unique cytoskeletal organization
351 of the sperm cells. The PT has a role of structural scaffold that surrounds sperm nucleus, and its protein
352 composition is crucial for correct sperm development. In this study, we used CRISPR/Cas9 gene editing
353 to establish *Cylc1-*, *Cylc2-* and *Cylc1/2*-deficient mouse lines to analyze the role of Cylicins. We
354 demonstrated that the loss of Cylicins impairs male fertility in mice by severely disturbing sperm head
355 architecture. The significance of our findings is supported by the identification of *CYLC1/2* variants in
356 an infertile patient who presents similar structural anomalies in sperm cells.

357 Detailed analysis of sperm development and morphology demonstrated that infertility of Cylicin-
358 deficient male mice is caused by anomalies of different sperm structures. The prominent loss of PT
359 integrity and calyx structure in the mature sperm lead to acrosome loosening and detachment from
360 the nuclear envelope. Furthermore, the shifting of the basal plate caused damage in the head-tail
361 connecting piece resulting in coiling of the flagellum and impaired swimming. Murine Cylicins are first
362 detected in the periacrosomal region of round spermatids and move to the postacrosomal region of
363 PT during spermatid elongation to finally localize to the calyx of mature sperm. This dynamic
364 localization pattern of Cylicins has been described in human, boar and bovine sperm as well [2, 14, 15].
365 Interestingly, other PT enriched proteins CCIN [12, 30, 7] and CPβ3/CPα3 move in the similar manner across
366 PT during spermiogenesis and are present in the calyx of mature sperm of various mammalian species.
367 This co-localization suggests the potential interaction between calyx proteins. Furthermore, CCIN [2, 12,
368 13] and CPβ3-CPα3 complex [16–18] are described as actin-binding proteins and porcine Cylc2 has been
369 shown to have a high affinity for F-actin as well [20]. The potential roles of F-actin during spermiogenesis
370 in mammals involve biogenesis of the acrosome [31] and its correct attachment to the outer nuclear
371 membrane of the spermatids [32] as well as removal of excess cytoplasm [33].

372 The loss of Cylicins caused acrosome detachment from NE starting from cap phase of the acrosome
373 biogenesis. Interestingly, loss of CCIN results in similar loosening of the acroplaxome from the outer
374 nuclear membrane [7]. Calicin is shown to be necessary for the IAM-PT-NE complex by establishing
375 bidirectional connections. Based on our findings, we conclude that both CCIN and Cylicins need to
376 interact in order to provide the 'molecular glue' necessary for the acrosome anchoring. Furthermore,
377 Cylicin-deficiency resulted in cytoplasmatic retention and bending of the midpiece, similarly to the
378 CPα3 mutant phenotype repro32/repro32 [34]. The CAPZ complex has been shown to regulate the actin
379 dynamics by preventing addition or loss of G-actin subunits to the ends of F-actin filaments [35]. Since
380 we demostrated that the loss of Cylicins resulted in mislocalization of both CCIN and CPα3, we
381 speculate that Cylicins have a crucial role in maintenance of the integrity of PT structure and thus are
382 required for proper function of PT proteins.

383 Other than morphological defects of the mature sperm PT, during spermiogenesis Cylicin-deficiency
384 results in excessive manchette elongation, its delayed disassembly as well as formation of abnormal
385 gaps in the PT at the level of perinuclear ring. The intra-manchette transport (IMT) of proteins from
386 the apical pole of the head to the base of the developing tail occurs during spermiogenesis [36]. The
387 malfunctions of the IMT can cause delay in manchette clearance and morphological defects of mature
388 sperm. Mouse models deficient for IMT proteins such as HOOK1 [25] CEP131 [37] and IFT88 [38] show
389 abnormal manchette elongation and delay in its clearance resulting in aberrant nuclear shape of the
390 sperm. Furthermore, the loss of HOOK1 results in head-tail connection and mid-piece anomalies such
391 as flipping of the head, basal plate defects and coiling of the tail similar to *Cylc2*-deficiency [39].
392 Furthermore, we observed wide gaps in the perinuclear ring during manchette elongation, suggesting
393 that Cylicins might have a role in maintenance of the contact between caudal and apical PT region and
394 its integrity.

395 Our evolutionary analysis of *Cylc1* and *Cylc2* genes across rodents and primates revealed that both
396 coding sequences are under purifying selection. Overall, the results reveal that *Cylc1* is under slightly
397 less conserved constraint than *Cylc2* leading to the hypothesis that loss of function in *Cylc1* might be
398 less severe and could be compensated for by *Cylc2* due to partial redundancy. This hypothesis is
399 supported by our finding that *Cylc1*-deficiency causes subfertility in male mice while the loss of both
400 *Cylc2* alleles results in male infertility. Furthermore, *in Cylc2*$^{+/-}$ male mice fertility was preserved while
401 *Cylc1*$^{-/Y}$ *Cylc2*$^{+/-}$ males were unable to sire offspring leading to the conclusion that the loss of one *Cylc2*
402 allele could be compensated by *Cylc1*, however at least two functional Cylicin alleles are required for
403 male fertility in mice.

404 In general, the evolutionary rate of C-terminal lysine rich region of both Cylicins seems to be highly
405 volatile between conserved and positively selected codon sites, while the lysine residues seem to be

strongly conserved. Changes in the C-terminal region, potentially affecting the length of the lysine rich domain, might have an adaptive advantage. Targeted positive selection on codon sites could also be a signature of co-evolution with a rapidly evolving interactor.

Sperm morphological defects and infertility observed in one patient with variants in both Cylicin genes points towards a requirement for human spermiogenesis and fertility. A defect in acrosome formation and the existence of variants in two out of three alleles in both *CYLC* genes is in line with the observations made in mice. The absence of CYLC1 confirmed through immunofluorescent staining indicates a functional impact of the missense variant on the CYLC1 protein. Furthermore, impaired CCIN localization was observed in patient M2270 as well, suggesting that PT has similar roles in human and rodents despite the differences in sperm head shape [40]. These results suggest that establishing mouse models deficient for Cylicin and other PT proteins might provide insights into mechanisms of human spermiogenesis and cytoskeletal regulation as well. However, with our data we cannot exclude the possibility that there is a discrepancy between mice and men and that the missense variant in *CYLC1* might alone be sufficient to cause the observed phenotype of M2270. The o/e ratios of both genes calculated within the gnomAD database rather indicate a stronger selective pressure on human *CYLC1* (0.08) than on *CYLC2* (0.84). Furthermore, the *CYLC1* variant affects an intolerant region within the protein sequence according to metadome [41], whereas the *CYLC2* variant is located in a region that is more tolerant to variation (Fig. S5). Therefore, we cannot definitively validate the hypothesis of an oligogenic disease in men as well.

The *CYLC2* missense variant is inherited by the father of M2270 (Fig. 5A) and, thus, not sufficient to cause infertility. However, the father reported difficulties to conceive naturally. Based on this one family, we cannot exclude an effect of pathogenic heterozygous *CYLC2* variants.

Overall, the identification and detailed characterization of further patients with variants in *CYLC1* and *CYLC2* is warranted to draw firm conclusions on the effect of variants in these genes on spermiogenesis and infertility.

Acknowledgment

This study was supported by a grant from the German Research Foundation (DFG) to HS (SCHO 503/23-1), SS (SCHN 1668/1-1) and FT (Clinical Research Unit ‚Male Germ Cells', CRU326). We are grateful to Gaby Beine, Angela Egert, Andrea Jäger, Greta Zech, Luisa Meier and Christina Burhöi for excellent technical assistance. We would like to thank the Core Facility for Microscopy of the Medical Faculty at the University of Bonn for providing support and instrumentation funded by the Deutsche Forschungsgemeinschaft (DFG, German Research Foundation, project number: 388169927)

Author Contributions

S.S. and H.S. conceived and designed the experiments. S.S. generated gene-edited mouse models. S.S., A.K. and M.M. analyzed Cylc1 and Cylc2 deficient mice. L.A. performed evolutionary analyses. A.K.D., S.A.K., C.B. and F.T. analyzed and provided exome sequencing data of infertile men. S.S., A.K. and H.S. were major contributors in writing the manuscript. All authors read and approved the final manuscript.

Figure legends

Figure 1: Loss of *Cylc1* or *Cylc2* results in impaired male fertility.

(A) Schematic representation of the *Cylc1* and *Cylc2* gene structure and targeting strategy for CRISPR/Cas9 mediated generation of *Cylc1*- and *Cylc2*- deficient alleles. Targeting sites of guide RNAs are depicted by red arrows. Genotyping primer binding sites are depicted by black arrows.
(B) Representative genotyping PCR of *Cylc1*- and *Cylc2*-deficient mice.
(C) Fertility analysis of Cylicin-deficient mice visualized by mean litter size and pregnancy rate (%) in comparison to wild type matings. Black dots represent mean values obtained for each male included in fertility testing. Columns represent mean values +/- standard deviation (SD). Total number of offspring per total number of pregnancies as well as total number of pregnancies per total number of plugs are depicted above each bar.
(D) Expression of *Cylc1* and *Cylc2* in testicular tissue of WT, *Cylc1*$^{-/y}$, *Cylc2*$^{+/-}$, *Cylc2*$^{-/-}$, *Cylc1* $^{-/y}$ *Cylc2*$^{+/-}$ and *Cylc1*$^{-/y}$ *Cylc2*$^{-/-}$ mice analyzed by qRT PCR.
(E) Immunofluorescent staining of testicular tissue and cauda epididymal sperm from WT, *Cylc1*$^{-/y}$, *Cylc2*$^{+/-}$, *Cylc2*$^{-/-}$, *Cylc1* $^{-/y}$ *Cylc2*$^{+/-}$ and *Cylc1*$^{-/y}$ *Cylc2*$^{-/-}$ males against CYLC1 and CYLC2. Cell nuclei were counterstained with DAPI. Scale bar: 5 µm.

Figure 2: Loss of Cylicins impairs spermiogenesis

(A) Testis weight [mg] and sperm count (x10^{7}) of WT, *Cylc1*$^{-/y}$, *Cylc2*$^{+/-}$, *Cylc2*$^{-/-}$, *Cylc1* $^{-/y}$ *Cylc2*$^{+/-}$ and *Cylc1*$^{-/y}$ *Cylc2*$^{-/-}$ males. Mean values +/- SD are shown; block dots represent data points for individual males.
(B) Comparable photographs of the testes of WT, *Cylc1*$^{-/y}$, *Cylc2*$^{+/-}$, *Cylc2*$^{-/-}$, *Cylc1* $^{-/y}$ *Cylc2*$^{+/-}$ and *Cylc1*$^{-/y}$ *Cylc2*$^{-/-}$ mice.
(C) PAS staining of testicular sections from WT, *Cylc1*$^{-/y}$, *Cylc2*$^{+/-}$, *Cylc2*$^{-/-}$, *Cylc1* $^{-/y}$ *Cylc2*$^{+/-}$ and *Cylc1*$^{-/y}$ *Cylc2*$^{-/-}$ mice. Scale bar: 100 µm.
(D) Epididymal sperm count (x10^{7}) of WT, *Cylc1*$^{-/y}$, *Cylc2*$^{+/-}$, *Cylc2*$^{-/-}$, *Cylc1* $^{-/y}$ *Cylc2*$^{+/-}$ and *Cylc1*$^{-/y}$ *Cylc2*$^{-/-}$ males. Mean values +/- SD are shown; block dots represent data points for individual males.
(E) Viability of the epididymal sperm stained with Eosin Nigrosine. Percentage of Eosin negative (viable) and Eosin positive (inviable) sperm is shown. Data represented as mean +/- SD.
(F) Motility of the epididymal sperm of WT, *Cylc1*$^{-/y}$, *Cylc2*$^{+/-}$, *Cylc2*$^{-/-}$, *Cylc1* $^{-/y}$ *Cylc2*$^{+/-}$ and *Cylc1*$^{-/y}$ *Cylc2*$^{-/-}$ males activated in TYH medium.
(G) Full and half-beat cycle plots of the flagellar beat are shown for WT and *Cylc2*$^{-/-}$ spermatozoa. Half beat cycle shows the stiffness of the midpiece (upper arrow) and high oscillations (lower arrow) in *Cylc2*$^{-/-}$ sperm in one direction of the beat.

Figure 3: Sperm morphology is severely altered in Cylicin deficient mice

(A) TEM micrographs of WT and *Cylc2*$^{-/-}$ epididymal sperm. Acrosome appears detached from the nucleus in *Cylc2*$^{-/-}$ sperm (green arrowheads) while the calyx is missing entirely (red arrowheads). The head-tail connecting piece shifted from the basal plate is shown by white arrowheads causing the looping of the flagellum and formation of a cytoplasmatic sac. Scale bar: 1 µm.
(B) Immunofluorescence staining of epididymal sperm acrosomes with PNA lectin (green) and tails with MITOred (red). Nuclei were counterstained with DAPI. Scale bar: 5 µm.
(C) Quantification of abnormal sperm of WT, *Cylc1*$^{-/y}$, *Cylc2*$^{+/-}$, *Cylc2*$^{-/-}$, *Cylc1* $^{-/y}$ *Cylc2*$^{+/-}$ and *Cylc1*$^{-/y}$ *Cylc2*$^{-/-}$ mice is shown. Acrosome aberrations and tail coiling were counted.

484 (D) Representative pictures of immunofluorescent staining against PT proteins CCIN (upper panel) and CAPZa3
485 (lower panel) in WT, *Cylc1*$^{-/y}$, *Cylc2*$^{+/-}$, *Cylc2*$^{-/-}$, *Cylc1* $^{-/y}$ *Cylc2*$^{+/-}$ and *Cylc1*$^{-/y}$ *Cylc2*$^{-/-}$ sperm. Nuclei were
486 counterstained with DAPI. Scale bar: 5 µm.
487 (E) Nuclear morphology analysis of WT, *Cylc1*$^{-/y}$, *Cylc2*$^{+/-}$, *Cylc2*$^{-/-}$, *Cylc1* $^{-/y}$ *Cylc2*$^{+/-}$ and *Cylc1*$^{-/y}$ *Cylc2*$^{-/-}$ sperm.
488 Number of cells analyzed for each genotype is shown.

489 PNA-FITC lectin immunofluorescence staining of the acrosome in testicular tissue of WT, *Cylc1*$^{-/y}$, *Cylc2*$^{+/-}$, *Cylc2*$^{-}$
490 $^{/-}$, *Cylc1* $^{-/y}$ *Cylc2*$^{+/-}$ and *Cylc1*$^{-/y}$ *Cylc2*$^{-/-}$ mice (green). Golgi phase of acrosome biogenesis at round spermatid stage
491 (I-IV) is visible in the upper panel. Middle panel shows cap phases on round spermatids (stage V-VIII). In the
492 bottom panel acrosomal phase is shown (stage IX-XI. Nuclei were counterstained with DAPI. Scale bar: 10 µm.

493 **Figure 4: *Cylc2* deficiency causes delay in manchette removal**

494 (A) Immunofluorescence staining of Tubulin manchette structure in the squash testis samples of WT, *Cylc1*$^{-/y}$,
495 *Cylc2*$^{+/-}$, *Cylc2*$^{-/-}$, *Cylc1* $^{-/y}$ *Cylc2*$^{+/-}$ and *Cylc1*$^{-/y}$ *Cylc2*$^{-/-}$ mice. Spermatids in different stages of spermiogenesis
496 were shown, for step-to-step comparison Scale bar: 5 µm.
497 (B) Co-staining of the manchette with HOOK1 and acrosome with PNA-lectin is shown in round, elongating and
498 elongated spermatids of WT (upper panel) and *Cylc2*$^{-/-}$ mice (lower panel). Schematic representation shows
499 acrosomal structure (green) and manchette filaments (red).
500 (C) TEM micrographs of testicular tissues of WT and *Cylc2*$^{-/-}$ mice. Single spermatids from step 6 to step 16 are
501 shown. nu: nucleus; av: acrosomal vesicle; pr: perinuclear ring; m: manchette microtubules cy: cytoplasm
502 Scale bar: 1 µm.
503 (D) TEM micrographs of degrading damaged spermatids in testicular sections of *Cylc2*$^{-/-}$ mice. Scale bar: 5 µm.

504 **Figure 5: Cylicins are required for human male fertility**

505 (A) Pedigree of patient M2270. His father (M2270_F) is carrier of the heterozygous *CYLC2* variant c.551G>A and
506 his mother (M2270_M) carries the X-linked *CYLC1* variant c.1720G>C in a heterozygous state. Asterisks (*)
507 indicate the location of the variants in *CYLC1* and *CYLC2* within the electropherograms.
508 (B) Immunofluorescence staining of CYLC1 in spermatozoa from healthy donor and patient M2270. In donor's
509 sperm cells CYLC1 localizes in the calyx, while patient's sperm cells are completely missing the signal.
510 (C) Bright field images of the spermatozoa from healthy donor and M2270 show visible head and tail
511 anomalies, coiling of the flagellum as well as headless spermatozoa who carry cytoplasmatic residues
512 without nuclei. Heads were counterstained with DAPI.
513 (D) Immunofluorescence staining of the CCIN in the human sperm cells. While in healthy sperm CCIN locates in
514 the funnel shaped calyx, sperm from M2270 show irregular expression of CCIN and lack of calyx.

515

516 **Table 1:** Semen analysis of the patient M2770 carrying variants in the *CYLC1* and *CYLC2* genes

	First visit	Second visit	WHO reference rang
Abstinence time [d]	4.0	5.0	
Volume [ml]	4.2	5.8	> 1.4
Concentration [Mill./ml]	10.5	16.3	> 16
Total sperm count [Mill.]	44.1	94.5	> 39
Vitality [%]	53	27	> 54
Motility			
a [%]	7	9	a + b >30
b [%]	5	4	
c [%]	19	8	
d [%]	69	79	
Morphology			
Normal [%]	2	2	> 4
Head defects [%]	99	99	
Midpiece defects [%]	63	59	
Flagella defects [%]	18	47	

517

518 **Table 2: Protospacer sequences**

Name	protospacer sequence (5´-3´)
Mm.Cas9.CYLC1.sg1	GGTTTATCCATACGTGAGT
Mm.Cas9.CYLC1.sg2	GGCTTAGGTGATGCTCTAAA
Mm.Cas9.CYLC2.1.AB	AAGGGAGAGTCGAAAAGCGT
Mm.Cas9.CYLC2.1.AF	GGATCCAAGGATAAAGTGTC

519

520 **Table 3: PCR primer sequences**

Cylc1	5´-3´	expected band size
Cylc1_F1	TATACACACAATCCACAATCTTGAAAT	WT: 427 bp
Cylc1_R1	TCACTTCAAAATCCAACTTGTCCT	KO: 264 bp
Cylc1_R2	TGCCTAGTATTTCAGGTTCCCC	
Cylc2		
Cylc2_F1	ACCACCATTATGGATGCACCG	WT: 376 bp
Cylc2_R1	AGTGTTTCTTGTGAGCTCGTTG	KO: 286 bp
Cylc2_R2	GGCTGAATCTTTACCCTTAGGT	

521

522 **Table 4: qRT primer sequences**

Name	Forward	reverse
Cylc1	GGGGAAAAATAAGCTCATGTGTAG	TTCAGGTTCCCCATTGGTTA
Cylc2	GCATTTCCCAAACCACCAAGG	AACGGATGGTCTCTCGGATATT
beta-actin	TGTTACCAACTGGGACGACA	GGGTGTTGAAGGTCTCAAA

523

524 **Table 5: Antibodies**

Antibody	**company**	**Order-number**	**Antigen**	**Dilution IF**
a-Tubulin	Merc Milipore (Billerica, USA)	16-232		1:1000
CapZa3	Progen	GP-SH4		1:500
Ccin	Progen	GP-SH3		1:500
Cylc1 (used for mouse)	Davids Biotechnology(Regensburg, Germany)	Custom made polyclonal antibody	AESRKSKNDERRKTLKIKFRGK and KDAKKEGKKKGKRESRKKR	1:1000 (sperm cells) 1:500 (testis tissue)
Cylc1 (used for human samples)	Santa Cruz	sc-166400		1:500
Cylc2	Davids Biotechnology(Regensburg, Germany)	Custom made polyclonal antibody	KSVGTHKSLASEKTKKEVK and ESGGEKAGSKKEAKDDKKDA	1:1000 (sperm cells) 1:500 (testis tissue)
Hook1	Proteintech	10871-1-AP		1:500

525

526 **Methods**

527 **Animals**

528 All animal experiments were conducted according to German law of animal protection and in
529 agreement with the approval of the local institutional animal care committees (Landesamt für Natur,
530 Umwelt und Verbraucherschutz, North Rhine-Westphalia, approval IDs: AZ84-02.04.2013.A429, AZ81-
531 02.04.2018.A369). *Cylc1*- and *Cylc2*-deficient mice were generated by CRISPR/Cas9 mediated gene-
532 editing in zygotes of the hybrid strain B6D2F1. Guide sequences are depicted in Table 2. For *Cylc1*, in

533 vitro transcribed sgRNAs (50 ng/µl each) and Cas9 mRNA (100 ng/µl) (Sigma-Aldrich, Taufkirchen,
534 Germany) were microinjected into the cytoplasm of zygotes as described previously [42]. *Cylc2* deficient
535 mice were generated by electroporation of ribonucleoprotein (RNP) complexes into zygotes using a
536 GenePulser II electroporation device (BioRad, Feldkirchen, Germany). For RNP formation, crRNA and
537 tracrRNA (IDT, Leuven, Belgium) were combined in duplex buffer (IDT) to a final concentration of 50
538 mM each and annealed (95°C, 5 min; cool down to room temperature with -0,2°C/sec.). For RNP
539 assembly, 4 µM Cas9 protein (IDT) and 2 µM of each annealed cr/tracr RNA were combined in Opti-
540 MEM media (Gibco 11058-021, Thermo Fisher, Carlsbad, USA) and incubated for 10 min at room
541 temperature. RNPs complexes were diluted 1:2 in Opti-MEM, supplemented with 30-40 zygotes in a
542 0.1 cm gene-pulser cuvette (BioRad) and electroporated (two 30 V square wave pulses, 2 ms pulse
543 length, 100 ms pulse interval). Recovered embryos were cultured over night at 37°C, 5% CO_2 in G-TL
544 medium (Vitrolife, Göteborg, Sweden) and transferred into the oviduct of pseudopregnant CB6F1
545 foster mice at 2-cell stage. Offspring were genotyped and gene-edited alleles were separated by
546 backcrossing of founder animals with C57Bl/6J mice. Established mouse lines were registered with
547 Mouse Genome Informatics: Cylc1^{em1Hsc} (MGI: 7341368), Cylc2^{em1Hsc} (MGI:6718280). Mouse lines were
548 maintained as congenic strains on C57Bl/6J background. For all analyses sexually mature males at the
549 age of 8-15 weeks, backcross generation ≥N3 were used.

550 **Genomic DNA extraction and genotyping**

551 Genomic DNA was extracted from biopsies using the HotShot method [43]. PCR reactions were
552 assembled according to the manufacturers protocol of the DreamTaq Green DNA Polymerase (Thermo
553 Fisher, EP0712) using gene specific primers listed in Table 3.

554 **Fertility analysis**

555 Males were mated 1:2/1:1 with C57Bl/6J females, which were checked daily for presence of a vaginal
556 plug indicative for successful copulation. Plug positive females were separated and pregnancies as well
557 as litter size were recorded.

558 **Sampling**

559 Mature sperm were obtained from the cauda epididymis in M2 medium (Merck) or PBS preheated at
560 37°C. Following several incisions of the cauda, sperm were retrieved by flush-out for 15-30 min. The
561 extracted sperm samples were washed in PBS, centrifuged (4000 rpm, 5 min, 4°C) and snap frozen. For
562 squash tubule samples, fresh testes were transferred to PBS and tubules were dissected as described
563 by [44]. Tubule sections were pressed on a slide, quickly frozen in liquid nitrogen and fixed in 90% ethanol
564 for 5 min.

565

566 **Semen analysis**

567 Sperm concentrations for at least 4 animals of each genotype were determined using a Neubauer
568 hemocytometer. Viability of sperm was determined by Eosin-Nigrosine staining as described previously
569 [45] for at least 3 animals per genotype. Sperm motility was analyzed referring to the WHO guidelines for
570 analysis of human semen. For all analyses at least 100 sperm per individual were analyzed and the
571 percentage of motile/immotile, viable/inviable sperm was calculated.

572 **Quantitative reverse transcription-polymerase chain reaction (qRT-PCR)**

573 RNA was extracted from the testis tissue with TRIzol (Life Technologies, Carlsbad, USA). RNA
574 concentrations and purity ratios were determined by NanoDrop ONE (Thermo Scientific)
575 measurements. qRT-PCR was performed as described previously [42], on ViiA 7 Real Time PCR System
576 (Applied Biosystems) using Maxima SYBR Green qPCR Mastermix (Thermo Fisher). Beta-actin was used
577 as a housekeeping gene for normalization. Primers used are shown in table 4.

578 **High-resolution microscopy of the flagellar beat**

579 Image sequences of mouse sperm were acquired using dark-field at an inverted microscope (IX71;
580 Olympus, Hamburg, Germany), equipped with a dark-field condenser and a high-speed camera (ORCA-
581 Flash4.0 V3, C13220-20 CU, Hamamatsu, Hamamatsu City, Japan). A 10x objective (NA 0.4, UPlanFL;
582 Olympus, Hamburg, Germany) with an additional 1.6x magnifying lens (Olympus, Hamburg, Germany)
583 that was inserted into the light path (final magnification: 16x) was applied. Image sequences were
584 recorded at a rate of 200 frames per second (fps). A custom-made observation chamber was used [21].
585 Sperm samples were diluted in THY buffer shortly before insertion of the suspension into the
586 observation chamber.

587 **Sperm nuclear morphology**

588 For the analysis of sperm nuclear morphology, epididymal sperm samples from 3 animals of each
589 genotype were fixed in methanol and acetic acid (3:1). The samples were spread onto a slide and
590 stained with 4',6-diamidino-2-phenylindole (DAPI) containing mounting medium (ROTImount
591 FluorCare DAPI (Carl Roth GmbH, Karlsruhe, Germany)). The sperm cells were imaged at 100x
592 magnification, using a Leica DM5500 B fluorescent microscope. At least 200 pictures were taken from
593 each group and analyzed using Nuclear Morphology software by [46] according to the developer's
594 instructions. The minimum detection area was set to 1.000 pixels while the maximum detection area
595 was 7.000 pixels.

596

597 **Histology**

598 Bouin fixed testis tissues were paraffinized, embedded and sectioned at 3-5 µm. For histological
599 analysis, the sections were deparaffinized and stained with Periodic acid Schiff (PAS staining). Stained
600 sections were imaged at 20x and 63x magnification under bright field using 5500 B microscope.

601 **Immunofluorescence**

602 Bouin fixed testis tissue sections were deparaffinized in Xylene and rehydrated in decreasing alcohol
603 to be used for immunohistochemical staining. Squash testis samples fixed in 90% EtOH were used for
604 the staining of a-Tubulin and HOOK1. For sperm immunofluorescence, mature sperm cells isolated
605 from cauda epididymis were fixed with methanol acetic acid (3:1), dropped on glass slides and air dried.
606 After washing in PBS twice, all samples were permeabilized using 0.1% Triton x100 for 10 min at room
607 temperature. The samples were then blocked with 5% BSA for 30 minutes, followed blocking with
608 normal horse serum (Vectorlabs, Burlingame, USA) for 30 minutes at room temperature. For tissue
609 sections, heat-activated antigen retrieval was performed using buffers at pH6. All primary antibodies
610 were incubated over night at 4°C. Antibodies and dilutions are listed in table 5. The respective
611 secondary antibodies were incubated for 1 h at room temperature using VectaFluor Labeling Kit
612 DyLight 488 and DyLight 594 (Vectorlabs, Burlingame, USA). All slides were mounted with DAPI
613 containing mounting medium (ROTImount FluorCare DAPI, Carl Roth).

614 For the analysis of acrosome biogenesis peanut agglutinin (PNA)-fluorescein isothiocyanite (FITC) Alexa
615 Fluor 488 conjugate (Molecular Probes, Invitrogen, Waltham, USA) was used on the Buin fixed testis
616 tissues. After permeabilization and blocking, the tissues were incubated with PNA-FITC 5 µg/ml for 30
617 minutes at room temperature. Mature sperm were fixed with paraformaldehyde (4%) for 20 min at
618 room temperature. After PBS washing, the sperm samples were incubated with 5 µg/ml PNA-FITC and
619 5 nM Mito Red (53271; Sigma Aldrich) for 30 min at room temperature. The slides were then mounted
620 with DAPI mount.

621 **Transmission electron microscopy**

622 For Transmission Electron Microscopy fresh epididymal sperm and testis tissue were used. After
623 washing with PBS, the samples were fixed in 3% glutaraldehyde at 4°C overnight. The samples were
624 then washed in 0.1 M cacodylate buffer and fixed again in 2% osmium tetroxide at 4% for 2 h. After
625 dehydration in an ascending ethanol row, the samples were contrasted in 70% ethanol 0.5% uranyl
626 acetate for 1.5h at 4°C. Samples were then washed in propylenoxide, three times for 10 minutes at
627 room temperature before embedding in Epon C at 70°C for 48h. Ultrathin sections were examined
628 using a Verios 460L microscope (FEI) with a STEM III-detector.

629

630 **Evolutionary analysis**

631 Evolutionary rates of mammalian Cylicin genes were analyzed according to [47]. Briefly, Cylc1 and Cylc2
632 nucleotide sequences were obtained from NCBI genbank and Ensembl genome browser. Phylogenetic
633 trees of considered species were built according to the "Tree of Life web project". The webPRANK
634 software was applied for codon-based alignment of orthologous gene sequences and results were
635 visualized using the ETE toolkit. To determine evolutionary rates of gene sequences across mammals,
636 for different clades and for individual codon sites, the codeml application implemented in the PAML
637 software was used [48, 49]. The M0 model served as basis for all performed analyses. Different codon
638 frequency settings were tested for the M0 model of each gene and the setting with the highest
639 likelihood was chosen. To test whether alternative models describe the selective constraints within a
640 dataset more precise than the M0 model, likelihood ratio-tests (LRT) were performed. Applied models
641 and LRTs are specified in Table S1.

642 **Study cohort and ethical approval**

643 The MERGE (**M**al**e R**eproductive **G**enomics study) cohort currently comprises over 2,030 men, mainly
644 recruited at the Centre of Reproductive Medicine and Andrology (CeRA) in Münster. The large majority
645 has severe spermatogenic failure, i.e. severe oligozoospermia (<5 Mill./ml sperm concentration),
646 crypto- or azoospermia. So far, only 35 cases were included because of notable sperm morphological
647 defects (≥5 Mill./ml sperm concentration, <4 % normal forms). Common causes for infertility such as
648 oncologic diseases, AZF deletions or chromosomal aberrations were ruled out in advance. Patients
649 with aetiologically still unexplained infertility underwent whole exome sequencing.

650 All participants gave written informed consent according to the protocols approved by the Ethics
651 Committee of the Medical Faculty Münster (Ref. No. MERGE: 2010-578-f-S) in accordance with the
652 Declaration of Helsinki in 1975.

653 **Whole exome sequencing and data analysis**

654 After DNA extraction from patients' peripheral blood lymphocytes WES was performed as previously
655 described [50]. WES data obtained from 2,066 infertile men was filtered for rare (≤ 0.01 minor allele
656 frequency, gnomAD) variants located within the coding sequence or the adjacent 15 bp of flanking
657 introns in *CYLC1* and *CYLC2*. Patients carrying only one variant in either of the gene were excluded. In
658 case of either bi-allelic *CYLC2* variants or a combination of *CYLC1* and *CYLC2* variants, the whole exome
659 dataset was screened to rule out other potential genetic causes. Variants detected in this study were
660 classified according to the guidelines by the American College of Medical Genetics and Genomics-
661 Association for Molecular Pathology (ACMG-AMP) [28] adapted to recent recommendations as outlined
662 in [51].

663 To rule out an alternative genetic cause for the patient's condition, his exome data was screened for
664 rare (MAF ≤ 0.01, gnomAD and in-house database), homozygous, X-linked or potentially compound
665 heterozygous high-impact variants (stop gain, start lost, stop lost, frameshift, splice site and splice
666 region as well as missense variants with CADD > 20) and rare, heterozygous LoF variants (stop gain,
667 start lost, stop lost, frameshift, splice site) without filtering for a specific set of genes. Respective genes
668 were screened for testis-expression and reports of infertility.

669

670 **Sanger sequencing**

671 Sanger sequencing with variant specific primers was conducted for validation and segregation
672 purposes. The primers to confirm the *CYLC1* (NM_021118.3) variant c.1720G>C p.(Glu574Gln) are
673 5'-ACTGATGCTGACTCTGAACCG-3' (forward) and 5'-CCTTCGAGTCACAAAGTTGTCA-3' (reverse). To
674 confirm the *CYLC2* (NM_001340.5) variant c.551G>A p.(Gly184Asp), the primers
675 5'-CTGTCGAGGTGGATTCTAAAGC-3' (forward) and 5'-TGCATCCTTCTTTGCATCCT-3' (reverse) were
676 used.

677 **Analysis of the human sperm samples**

678 Human ejaculate samples from healthy donor and patient M2270, were analyzed according to WHO
679 guidelines prior to washing in buffer and centrifuged (1000 rpm, 20 min). The cells were fixed in
680 methanol and acetic acid (3:1) and used for immunofluorescence staining. Samples were dropped on
681 slides and permeabilized with 0.1% Triton x100. After blocking with 5% BSA for 30 min, slides were
682 incubated with primary CCIN or CYLC1 antibodies (concentrations shown in Table 3) for 3 h at room
683 temperature. Secondary antibodies were incubated for 1 h, followed by mounting with DAPI
684 containing medium.

685 **Statistics**

686 For all analyses mean values +/- SD were calculated. Statistical significance was determined by One-
687 way ANNOVA analyses using Bonferroni correction.

688

689 **References**

690 1. Teves, M.E., Roldan, E.R.S., Krapf, D., Strauss, J.F., Bhagat, V., and Sapao, P. (2020). Sperm
691 Differentiation: The Role of Trafficking of Proteins. International journal of molecular sciences
692 *21*.
693 2. Longo, F.J., Krohne, G., and Franke, W.W. (1987). Basic proteins of the perinuclear theca of
694 mammalian spermatozoa and spermatids: a novel class of cytoskeletal elements. The Journal of
695 cell biology *105,* 1105–1120.

3. Longo, F.J., and Cook, S. (1991). Formation of the perinuclear theca in spermatozoa of diverse mammalian species: relationship of the manchette and multiple band polypeptides. Molecular reproduction and development *28,* 380–393.
4. Oko, R., and Sutovsky, P. (2009). Biogenesis of sperm perinuclear theca and its role in sperm functional competence and fertilization. Journal of reproductive immunology *83,* 2–7.
5. Oko, R., and Maravei, D. (1995). Distribution and possible role of perinuclear theca proteins during bovine spermiogenesis. Microscopy research and technique *32,* 520–532.
6. Zhang, M., Chiozzi, R.Z., Skerrett-Byrne, D.A., Veenendaal, T., Klumperman, J., Heck, A.J.R., Nixon, B., Helms, J.B., Gadella, B.M., and Bromfield, E.G. (2022). High Resolution Proteomic Analysis of Subcellular Fractionated Boar Spermatozoa Provides Comprehensive Insights Into Perinuclear Theca-Residing Proteins. Frontiers in cell and developmental biology *10,* 836208.
7. Zhang, X.-Z., Wei, L.-L., Jin, H.-J., Zhang, X.-H., and Chen, S.-R. (2022). The perinuclear theca protein Calicin helps shape the sperm head and maintain the nuclear structure in mice. Cell reports *40,* 111049.
8. Hamilton, L.E., Lion, M., Aguila, L., Suzuki, J., Acteau, G., Protopapas, N., Xu, W., Sutovsky, P., Baker, M., and Oko, R. (2021). Core Histones Are Constituents of the Perinuclear Theca of Murid Spermatozoa: An Assessment of Their Synthesis and Assembly during Spermiogenesis and Function after Gametic Fusion. International journal of molecular sciences *22*.
9. Sutovsky, P., Manandhar, G., Wu, A., and Oko, R. (2003). Interactions of sperm perinuclear theca with the oocyte: implications for oocyte activation, anti-polyspermy defense, and assisted reproduction. Microscopy research and technique *61,* 362–378.
10. Herrada, G., and Wolgemuth, D.J. (1997). The mouse transcription factor Stat4 is expressed in haploid male germ cells and is present in the perinuclear theca of spermatozoa. Journal of cell science *110 (Pt 14),* 1543–1553.
11. Tovich, P.R., and Oko, R.J. (2003). Somatic histones are components of the perinuclear theca in bovine spermatozoa. The Journal of biological chemistry *278,* 32431–32438.
12. Paranko, J., Longo, F., Potts, J., Krohne, G., and Franke, W.W. (1988). Widespread occurrence of calicin, a basic cytoskeletal protein of sperm cells, in diverse mammalian species. Differentiation; research in biological diversity *38,* 21–27.
13. Bülow, M. von, Heid, H., Hess, H., and Franke, W.W. (1995). Molecular nature of calicin, a major basic protein of the mammalian sperm head cytoskeleton. Experimental cell research *219,* 407–413.
14. Hess, H., Heid, H., and Franke, W.W. (1993). Molecular characterization of mammalian cylicin, a basic protein of the sperm head cytoskeleton. The Journal of cell biology *122,* 1043–1052.
15. Hess, H., Heid, H., Zimbelmann, R., and Franke, W.W. (1995). The protein complexity of the cytoskeleton of bovine and human sperm heads: the identification and characterization of cylicin II. Experimental cell research *218,* 174–182.
16. Bülow, M. von, Rackwitz, H.R., Zimbelmann, R., and Franke, W.W. (1997). CP beta3, a novel isoform of an actin-binding protein, is a component of the cytoskeletal calyx of the mammalian sperm head. Experimental cell research *233,* 216–224.
17. Hurst, S., Howes, E.A., Coadwell, J., and Jones, R. (1998). Expression of a testis-specific putative actin-capping protein associated with the developing acrosome during rat spermiogenesis. Molecular reproduction and development *49,* 81–91.
18. Tanaka, H., Yoshimura, Y., Nishina, Y., Nozaki, M., Nojima, H., and Nishimune, Y. (1994). Isolation and characterization of cDNA clones specifically expressed in testicular germ cells. FEBS Letters *355,* 4–10.
19. Heid, H., Figge, U., Winter, S., Kuhn, C., Zimbelmann, R., and Franke, W. (2002). Novel actin-related proteins Arp-T1 and Arp-T2 as components of the cytoskeletal calyx of the mammalian sperm head. Experimental cell research *279,* 177–187.

745 20. Rousseaux-Prévost, R., Lécuyer, C., Drobecq, H., Sergheraert, C., Dacheux, J.-L., and Rousseaux,
746 J. (2003). Characterization of boar sperm cytoskeletal cylicin II as an actin-binding protein.
747 Biochemical and biophysical research communications *303,* 182–189.
748 21. Hansen, J.N., Rassmann, S., Jikeli, J.F., and Wachten, D. (2018). SpermQ¯A Simple Analysis
749 Software to Comprehensively Study Flagellar Beating and Sperm Steering. Cells *8*.
750 22. Gadadhar, S., Alvarez Viar, G., Hansen, J.N., an Gong, Kostarev, A., Ialy-Radio, C., Leboucher, S.,
751 Whitfield, M., Ziyyat, A., and Touré, A., et al. (2021). Tubulin glycylation controls axonemal
752 dynein activity, flagellar beat, and male fertility. Science (New York, N.Y.) *371*.
753 23. Wear, M.A., and Cooper, J.A. (2004). Capping protein: new insights into mechanism and
754 regulation. Trends in biochemical sciences *29,* 418–428.
755 24. Okuda, H., DeBoer, K., O'Connor, A.E., Merriner, D.J., Jamsai, D., and O'Bryan, M.K. (2017).
756 LRGUK1 is part of a multiprotein complex required for manchette function and male fertility.
757 FASEB journal : official publication of the Federation of American Societies for Experimental
758 Biology *31,* 1141–1152.
759 25. Mendoza-Lujambio, I., Burfeind, P., Dixkens, C., Meinhardt, A., Hoyer-Fender, S., Engel, W., and
760 Neesen, J. (2002). The Hook1 gene is non-functional in the abnormal spermatozoon head shape
761 (azh) mutant mouse. Human molecular genetics *11,* 1647–1658.
762 26. Ng, P.C., and Henikoff, S. (2003). SIFT: Predicting amino acid changes that affect protein
763 function. Nucleic acids research *31,* 3812–3814.
764 27. Adzhubei, I.A., Schmidt, S., Peshkin, L., Ramensky, V.E., Gerasimova, A., Bork, P., Kondrashov,
765 A.S., and Sunyaev, S.R. (2010). A method and server for predicting damaging missense
766 mutations. Nature methods *7,* 248–249.
767 28. Richards, S., Aziz, N., Bale, S., Bick, D., Das, S., Gastier-Foster, J., Grody, W.W., Hegde, M., Lyon,
768 E., and Spector, E., et al. (2015). Standards and guidelines for the interpretation of sequence
769 variants: a joint consensus recommendation of the American College of Medical Genetics and
770 Genomics and the Association for Molecular Pathology. Genetics in medicine : official journal of
771 the American College of Medical Genetics *17,* 405–424.
772 29. World Health Organization (2021). WHO laboratory manual for the examination and processing
773 of human semen (Geneva).
774 30. Lécuyer, C., Dacheux, J.L., Hermand, E., Mazeman, E., Rousseaux, J., and Rousseaux-Prévost, R.
775 (2000). Actin-binding properties and colocalization with actin during spermiogenesis of
776 mammalian sperm calicin. Biology of reproduction *63,* 1801–1810.
777 31. Welch, J.E., and O'Rand, M.G. (1985). Identification and distribution of actin in spermatogenic
778 cells and spermatozoa of the rabbit. Developmental biology *109,* 411–417.
779 32. Russell, L.D., Weber, J.E., and Vogl, A. (1986). Characterization of filaments within the
780 subacrosomal space of rat spermatids during spermiogenesis. Tissue & cell *18,* 887–898.
781 33. Russell, L.D. (1979). Spermatid-Sertoli tubulobulbar complexes as devices for elimination of
782 cytoplasm from the head region late spermatids of the rat. The Anatomical record *194,* 233–
783 246.
784 34. Geyer, C.B., Inselman, A.L., Sunman, J.A., Bornstein, S., Handel, M.A., and Eddy, E.M. (2009). A
785 missense mutation in the Capza3 gene and disruption of F-actin organization in spermatids of
786 repro32 infertile male mice. Developmental biology *330,* 142–152.
787 35. Wear, M.A., Yamashita, A., Kim, K., Maéda, Y., and Cooper, J.A. (2003). How Capping Protein
788 Binds the Barbed End of the Actin Filament. Current Biology *13,* 1531–1537.
789 36. Lehti, M.S., and Sironen, A. (2016). Formation and function of the manchette and flagellum
790 during spermatogenesis. Reproduction (Cambridge, England) *151,* R43-54.
791 37. Hall, E.A., Keighren, M., Ford, M.J., Davey, T., Jarman, A.P., Smith, L.B., Jackson, I.J., and Mill, P.
792 (2013). Acute versus chronic loss of mammalian Azi1/Cep131 results in distinct ciliary
793 phenotypes. PLoS genetics *9,* e1003928.

38. Kierszenbaum, A.L., Rivkin, E., Tres, L.L., Yoder, B.K., Haycraft, C.J., Bornens, M., and Rios, R.M. (2011). GMAP210 and IFT88 are present in the spermatid golgi apparatus and participate in the development of the acrosome-acroplaxome complex, head-tail coupling apparatus and tail. Developmental dynamics : an official publication of the American Association of Anatomists *240,* 723–736.
39. Mochida, K., Tres, L.L., and Kierszenbaum, A.L. (1999). Structural and biochemical features of fractionated spermatid manchettes and sperm axonemes of theAzh/Azh mutant mouse. Molecular reproduction and development *52,* 434–444.
40. Courtot, A.M. (1991). Presence and localization of the 60 KD calicin in human spermatozoa presenting postacrosomal sheath defects: preliminary results. Molecular reproduction and development *28,* 272–279.
41. Wiel, L., Baakman, C., Gilissen, D., Veltman, J.A., Vriend, G., and Gilissen, C. (2019). MetaDome: Pathogenicity analysis of genetic variants through aggregation of homologous human protein domains. Human mutation *40,* 1030–1038.
42. Schneider, S., Balbach, M., Jan, F.J., Fietz, D., Nettersheim, D., Jostes, S., Schmidt, R., Kressin, M., Bergmann, M., and Wachten, D., et al. (2016). Re-visiting the Protamine-2 locus: deletion, but not haploinsufficiency, renders male mice infertile. Scientific reports *6,* 36764.
43. Truett, G.E., Heeger, P., Mynatt, R.L., Truett, A.A., Walker, J.A., and Warman, M.L. (2000). Preparation of PCR-quality mouse genomic DNA with hot sodium hydroxide and tris (HotSHOT). BioTechniques *29,* 52, 54.
44. Kotaja, N., Lin, H., Parvinen, M., and Sassone-Corsi, P. (2006). Interplay of PIWI/Argonaute protein MIWI and kinesin KIF17b in chromatoid bodies of male germ cells. Journal of cell science *119,* 2819–2825.
45. Schneider, S., Shakeri, F., Trötschel, C., Arévalo, L., Kruse, A., Buness, A., Poetsch, A., Steger, K., and Schorle, H. (2020). Protamine-2 Deficiency Initiates a Reactive Oxygen Species (ROS)-Mediated Destruction Cascade during Epididymal Sperm Maturation in Mice. Cells *9*.
46. Skinner, B.M., Rathje, C.C., Bacon, J., Johnson, E.E.P., Larson, E.L., Kopania, E.E.K., Good, J.M., Yousafzai, G., Affara, N.A., and Ellis, P.J.I. (2019). A high-throughput method for unbiased quantitation and categorization of nuclear morphology†. Biology of reproduction *100,* 1250–1260.
47. Lüke, L., Tourmente, M., and Roldan, E.R.S. (2016). Sexual Selection of Protamine 1 in Mammals. Molecular biology and evolution *33,* 174–184.
48. Yang, Z. (1997). PAML: a program package for phylogenetic analysis by maximum likelihood. Computer applications in the biosciences : CABIOS *13,* 555–556.
49. Yang, Z. (2007). PAML 4: phylogenetic analysis by maximum likelihood. Molecular biology and evolution *24,* 1586–1591.
50. Wyrwoll, M.J., Temel, Ş.G., Nagirnaja, L., Oud, M.S., Lopes, A.M., van der Heijden, G.W., Heald, J.S., Rotte, N., Wistuba, J., and Wöste, M., et al. (2020). Bi-allelic Mutations in M1AP Are a Frequent Cause of Meiotic Arrest and Severely Impaired Spermatogenesis Leading to Male Infertility. American journal of human genetics *107,* 342–351.
51. Wyrwoll, M.J., Köckerling, N., Vockel, M., Dicke, A.-K., Rotte, N., Pohl, E., Emich, J., Wöste, M., Ruckert, C., and Wabschke, R., et al. (2022). Genetic Architecture of Azoospermia-Time to Advance the Standard of Care. European urology.

Figure 1

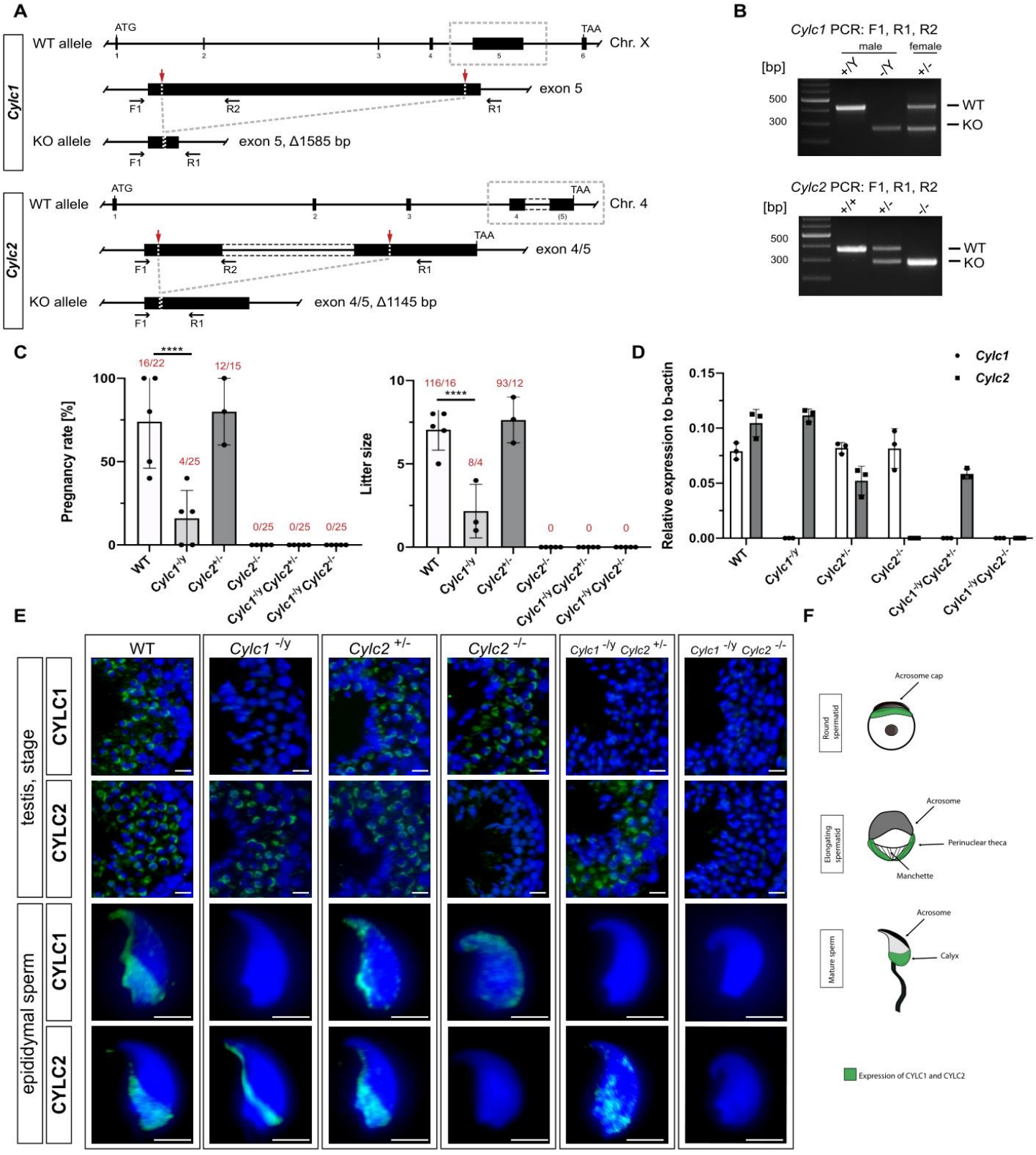
A
Cylc1
WT allele
ATG
TAA
Chr. X
exon 5
KO allele
exon 5, Δ1585 bp
F1
R2
R1
Cylc2
WT allele
ATG
TAA
Chr. 4
exon 4/5
KO allele
exon 4/5, Δ1145 bp
B
Cylc1 PCR: F1, R1, R2
male
female
[bp]
500
300
WT
KO
Cylc2 PCR: F1, R1, R2
C
Pregnancy rate [%]
16/22
4/25
12/15
0/25
0/25
0/25
Litter size
116/16
8/4
93/12
0
0
0
WT
Cylc1-/y
Cylc2+/-
Cylc2-/-
Cylc1-/y Cylc2+/-
Cylc1-/y Cylc2-/-
D
Relative expression to b-actin
Cylc1
Cylc2
E
WT
Cylc1 -/y
Cylc2 +/-
Cylc2 -/-
Cylc1 -/y Cylc2 +/-
Cylc1 -/y Cylc2 -/-
testis, stage
CYLC1
CYLC2
epididymal sperm
CYLC1
CYLC2
F
Round spermatid
Acrosome cap
Elongating spermatid
Acrosome
Perinuclear theca
Manchette
Mature sperm
Acrosome
Calyx
Expression of CYLC1 and CYLC2

Figure 2

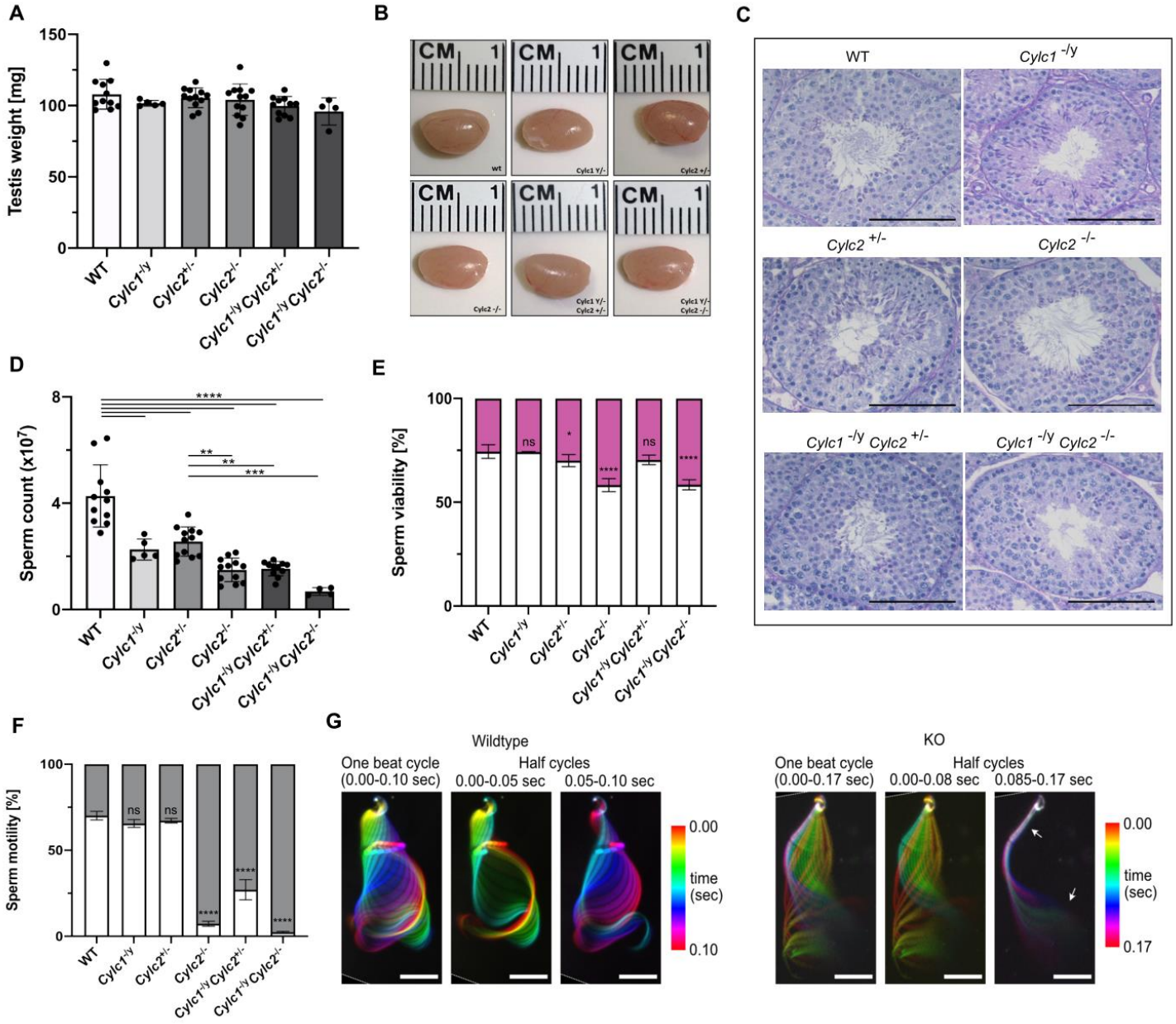
A
Testis weight [mg]
150
100
50
0
WT
Cylc1-/y
Cylc2+/-
Cylc2-/-
Cylc1-/y Cylc2+/-
Cylc1-/y Cylc2-/-
B
CM 1
wt
Cylc1 Y/-
Cylc2 +/-
Cylc2 -/-
Cylc1 Y/- Cylc2 +/-
Cylc1 Y/- Cylc2 -/-
C
WT
Cylc1 -/y
Cylc2 +/-
Cylc2 -/-
Cylc1 -/y Cylc2 +/-
Cylc1 -/y Cylc2 -/-
D
Sperm count (x10^7)
8
4
0
****
**
**
***
E
Sperm viability [%]
100
50
0
ns
*
****
ns
****
F
Sperm motility [%]
100
50
0
ns
ns
****
****
****
G
Wildtype
One beat cycle (0.00-0.10 sec)
Half cycles
0.00-0.05 sec
0.05-0.10 sec
0.00
time (sec)
0.10
KO
One beat cycle (0.00-0.17 sec)
Half cycles
0.00-0.08 sec
0.085-0.17 sec
0.00
time (sec)
0.17

Figure 3

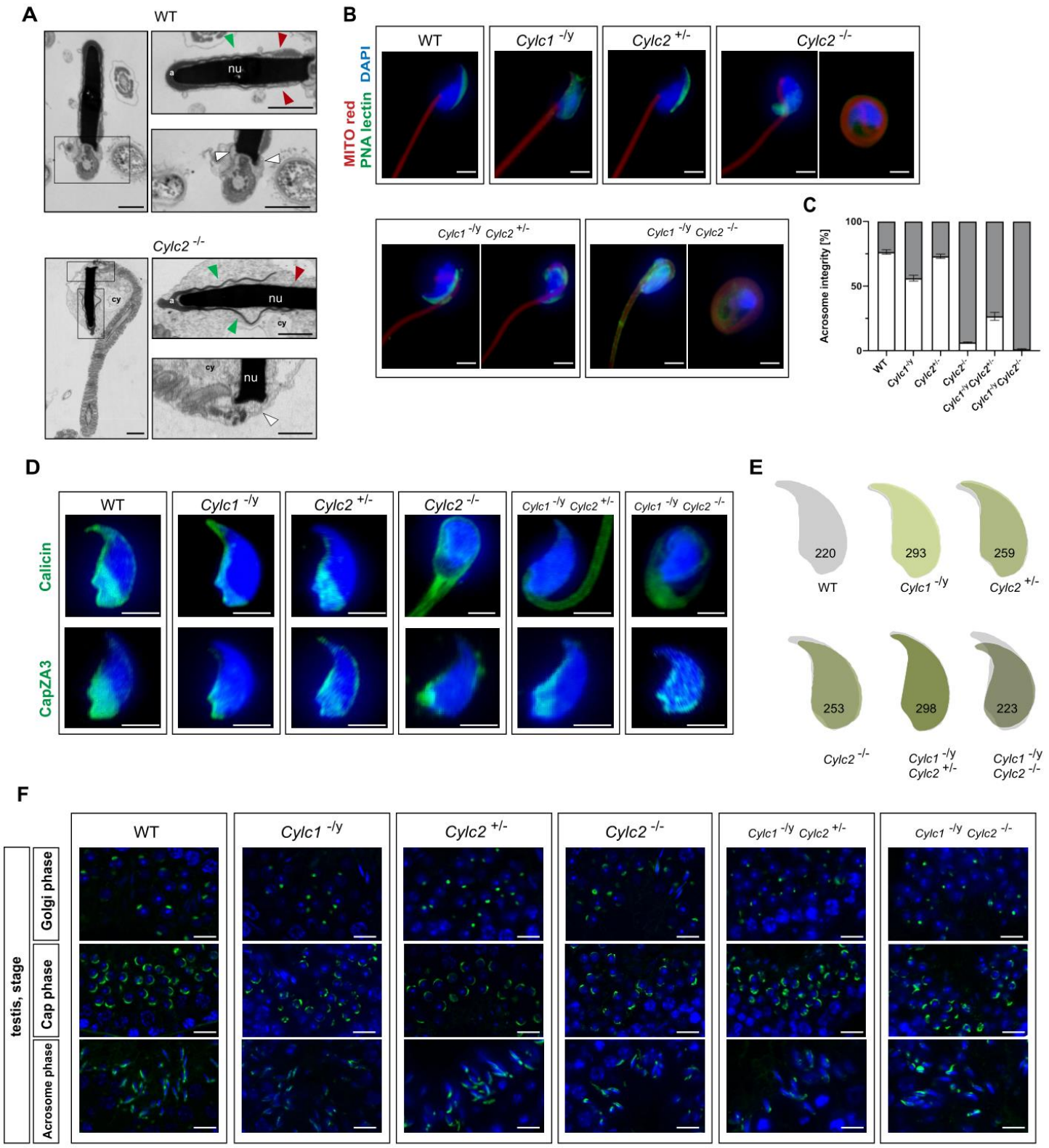
A
WT
nu
a
Cylc2 -/-
cy
B
WT
Cylc1 -/y
Cylc2 +/-
Cylc2 -/-
DAPI
MITO red
PNA lectin
Cylc1 -/y Cylc2 +/-
Cylc1 -/y Cylc2 -/-
C
Acrosome integrity [%]
100
50
0
WT
Cylc1-/y
Cylc2+/-
Cylc2-/-
Cylc1-/yCylc2+/-
Cylc1-/yCylc2-/-
D
Calicin
CapZA3
E
220
293
259
253
298
223
F
testis, stage
Golgi phase
Cap phase
Acrosome phase

Figure 4

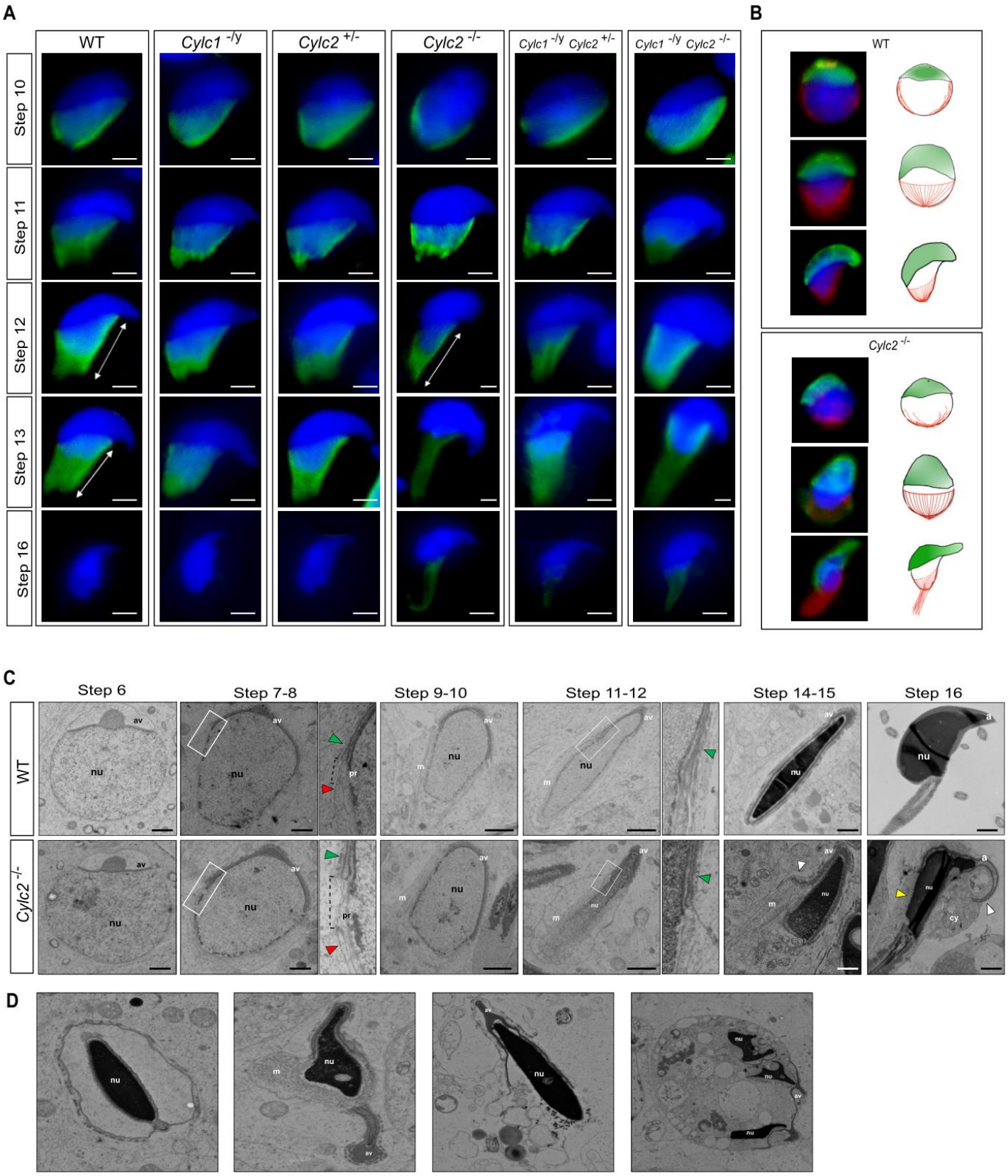
A
WT
Cylc1 -/y
Cylc2 +/-
Cylc2 -/-
Cylc1 -/y Cylc2 +/-
Cylc1 -/y Cylc2 -/-
Step 10
Step 11
Step 12
Step 13
Step 16
B
WT
Cylc2 -/-
C
Step 6
Step 7-8
Step 9-10
Step 11-12
Step 14-15
Step 16
WT
Cylc2 -/-
av
nu
m
pr
a
cy
D

Figure 5

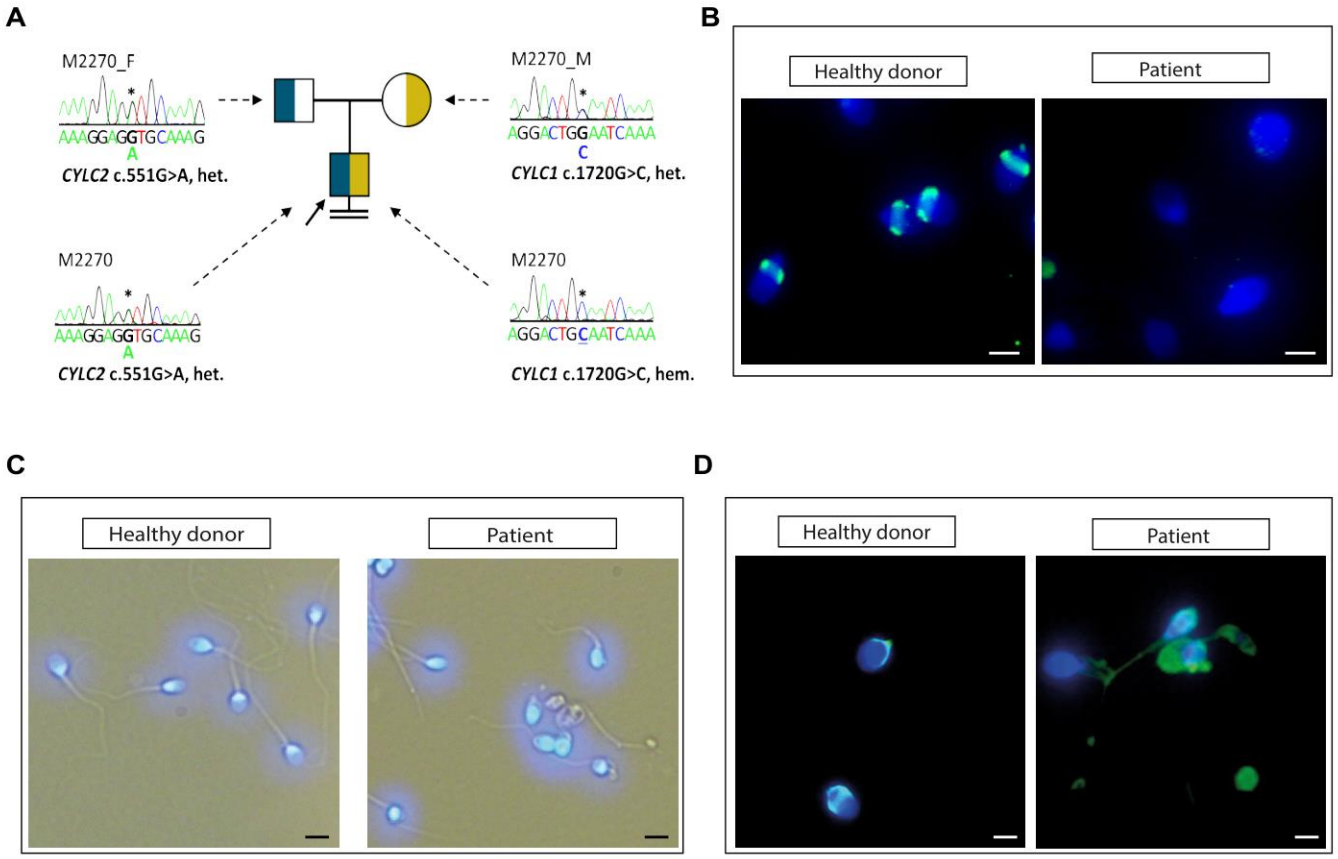
A
M2270_F
AAAGGAGGTGCAAAG
A
CYLC2 c.551G>A, het.
M2270_M
AGGACTGGAATCAAA
C
CYLC1 c.1720G>C, het.
M2270
AAAGGAGGTGCAAAG
A
CYLC2 c.551G>A, het.
M2270
AGGACTGCAATCAAA
CYLC1 c.1720G>C, hem.
B
Healthy donor
Patient
C
Healthy donor
Patient
D
Healthy donor
Patient